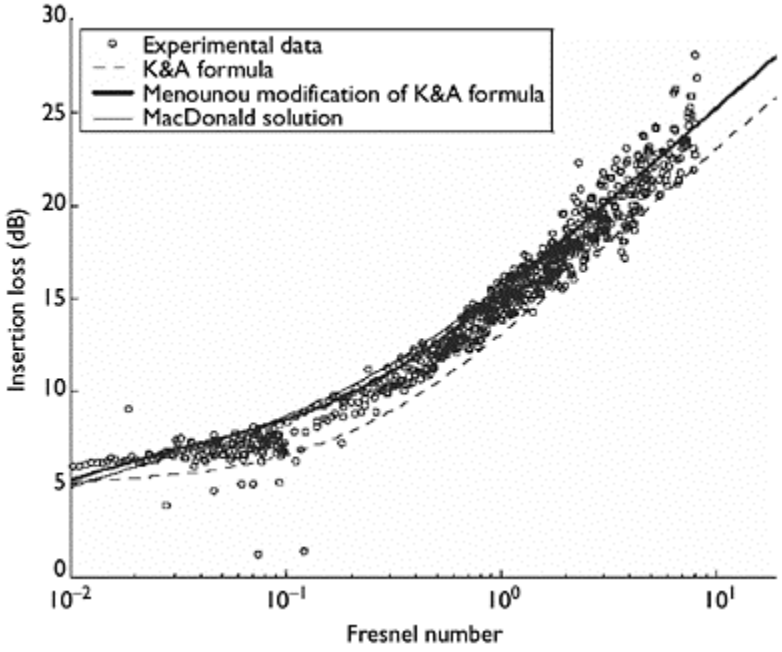

Figure 9.10 Comparison between laboratory data and predictions of the Kurze and Anderson (K&A) empirical formula. Predictions of Menounou's modification on the Kurze and Anderson formula is also shown. The insertion loss of the thin half plane is plotted against the Fresnel number, N_1.

The term Att_s is a function of N_1 which is a measure of the relative position of the receiver from the source. The second term depends on the ratio of N_2/N_1. It is a measure of the proximity of either the source or the receiver from the half plane. The third term is only significant when N_1 is small. It is a measure of the proximity of the receiver to the shadow boundary. The last term is a function of the ratio R'/R_1 which is used to account for the diffraction effect due to spherical incident waves.

Figure 9.10 shows the predicted attenuation according to the Kurze and Anderson formula and the Menounou modification. Again, both formulae appear to give predictions in agreement with the data for a thin screen.

9.4 The sound attenuation by a thin barrier on an impedance ground

The diffraction of sound by a semi-infinite rigid plane is a classical problem in wave theory and dates back to the nineteenth century. There was renewed interest in the problem between the 1970s and early 1980s in connection with the acoustic effectiveness

of outdoor noise barriers. Since outdoor noise barriers are always on the ground, the attenuation is different from that discussed in sections 9.2 and 9.3 for a semi-infinite plane screen. Extensive literature reviews on the pertinent theory and details on precise experimental studies have been carried out by Embleton and his co-workers [27, 28].

Figure 9.11 shows the situation of interest. A source S_g is located at the left side of the barrier, a receiver R_g at the right side of the barrier and O is the diffraction point on the barrier edge. The sound reflected from the ground surface can be described by the source's 'mirror' image, S_i. On the receiver side, sound waves will also be reflected from the ground and this effect can be considered in terms of the image of the receiver, R_i. The pressure at the receiver is the sum of four terms which correspond to the sound paths S_gOR_g, S_iOR_g, S_gOR_i and S_iOR_i.

If the surface is a perfectly reflecting ground, the total sound field is the sum of the diffracted fields of these four paths,

$$P_T = P_1 + P_2 + P_3 + P_4 \tag{9.33}$$

where

$$P_1 = P(S_g, R_g, O), \tag{9.34a}$$

$$P_2 = P(S_i, R_g, O), \tag{9.34b}$$

$$P_3 = P(S_g, R_i, O), \tag{9.34c}$$

$$P_4 = P(S_g, R_i, O), \tag{9.34d}$$

and $P(S, R, O)$ is the diffracted sound field due to a thin barrier for given positions of source S, receiver R and the point of diffraction at the barrier edge O.

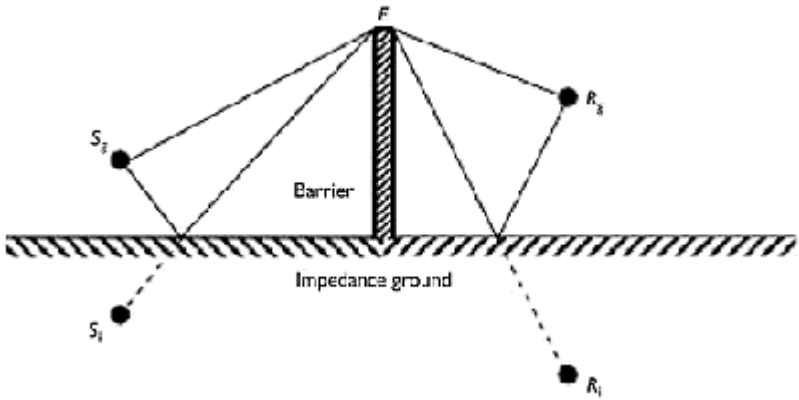

Figure 9.11 Ray paths for a thin barrier placed on the ground between the source and receiver.

If the ground has a finite im pedance (such as grass or a porous road surface) then the pressure corresponding to rays reflected from these surfaces will need to be multiplied by the appropriate spherical wave reflection coefficient(s) to allow for the change in phase and amplitude of the wave on reflection as follows:

$$P_T = P_1 + Q_s P_2 + Q_R P_3 + Q_s Q_R P_4, \tag{9.35}$$

where Q_s and Q_R are the spherical wave reflection co efficients at the source and receiver side, respectively. The spherical wave reflec tion coefficients can be calculated according to (2.40c) for different types of ground surfaces and source/receiver geometries.

For a given source and receiver position, the acoustic performance of the barrier on the ground is normally assessed by use of either the excess attenuation (EA) or the insertion loss (IL). They are defined as follows:

$$EA = SPL_b - SPL_f \tag{9.36a}$$

$$IL = SPL_b - SPL_g, \tag{9.36b}$$

where SPL_f is the free field noise level, SPL_g is the noise level with the ground present and SPL_b is the noise level with the barrier and ground present. Note that in the absence of a refl ecting ground, t he numerical value of EA (see al so Att defined by (9.21) in section 9.2.3) is the same as IL. If th e calculation is carried out in terms of amplitude only, as descri bed in [19], then the attenuation Att_n for each ray path can be directly determined from the appropriate Fresnel number F_n for that path. The excess attenuation of the barrier on a rigid ground is then given by

$$EA = 10\log(10^{-|Att_1/10|} + 10^{-|Att_2/10|} + 10^{-|Att_3/10} + 10^{-|Att_4/10|}). \tag{9.37}$$

The attenuation for each path can either be calculated by the empirical or analytical formulas listed in sections 9.2 and 9.3 depending on the complexity of the model and the required accuracy. If the calculation demands an accurate estimation on both the amplitude and phase of the diffracted waves, then the MacDonald solution or the Hadden and Pierce solution should be used although the latter solution will give a more accurate solution for both source and receiver locating very close to the barrier [28]. Nevertheless, the former solution is equally accurate for most practical applications where both the source and receiver are far from the barrier edge.

Figure 9.12(a) displays predicted insertion loss spectra for propagation from a point source for the source-receiver-barrier geometry indicated. The sound pressure was calculated using the four sound paths described above and the MacDonald expression (9.9). Curves plotted with a thin line is for a rigid ground surface and a dashed line is for an absorbing surface such as grassland. For the grassland impedance, the Delany and Bazley one-parameter model with an effective flow resistivity of 300 kPa s m^{-2} has been used. The oscillations are due to interference between the sound waves along the four ray paths considered. The curve plotted as a thick line is the result using Maekawa's method to determine the attenuation of each ray path. The total insertion loss is obtained by summing all four paths incoherently by assuming that the point source is located above a rigid ground. The same method is used to predict the insertion loss above the absorbing surface. The predicted results (dotted line) are presented in Figure 9.12(a). Neither of the incoherent predictions oscillates since the phases of the waves are not considered. Nevertheless, these lines give a reasonable approximation to the results of more complex calculations [29].

Figure 9.12(b) shows results for a similar geometry except that in this case a line of *incoherent* point sources, separated by approximately 1.5 m along the nominal road line, has been assumed and the calculation has been carried out for each source. The averaging over all the predictions for the different sources has smoothed the curves. Note that the IL for the grassland case becomes negative around 500 Hz indicating that the sound absorption due to the grass is greater than the screening effect of the barrier for these conditions.

In both Figure 9.12(a) and (b), the height of the barrier is taken as 3 m. The source is assumed to be 5 m from the barrier and 0.3 m above the ground. The receiver is assumed to be 30 m from the barrier and 1.2 m above the ground.

Lam and Roberts [30] have suggested a relatively simple approach for modelling full wave effects. In their model the amplitude of the diffracted wave, Att1, may be calculated using a method such as that described in section 9.3. However, the phase of the wave at the receiver is calculated from the path length via the top of the screen assuming a phase change in the diffracted wave of $\pi/4$. It is assumed that the phase change is constant for all source, barrier and receiver heights and locations. For example, the diffracted wave for the path S_gOR_g would be given by

$$P_1 = \mathrm{Att}_1 e^{i[k(r_0+r_r)+\pi/4]}. \tag{9.38}$$

It is straightforward to compute the contributions for other diffracted paths and hence the total sound field can be calculated through the use of (9.35) for impedance ground and (9.33) for a hard ground. This approach provides a reasonable approximation for many conditions normally encountered in practical barrier situations where source and receiver are many wavelengths from the barrier and the receiver is in the shadow zone.

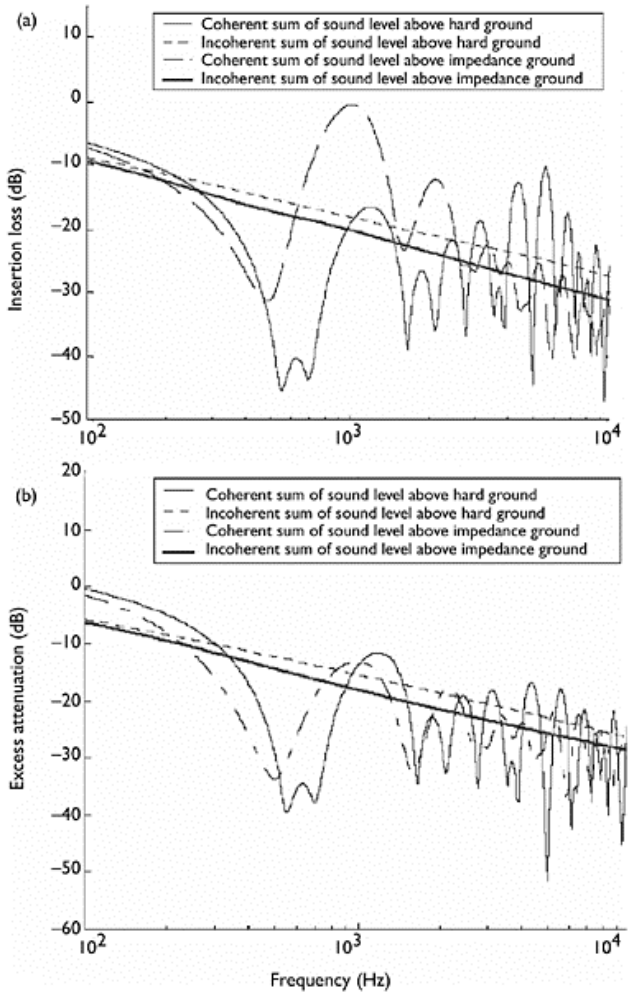

Figure 9.12 Comparison of predictions resulting from summing the contributions of different ray paths incoherently and coherently for the sound field (a) insertion loss due to a point source and (b) excess attenuation from a coherent line source behind an outdoor noise barrier placed on a ground surface.

The scheme works well for a barrier located on a hard ground but less so if the ground has finite impedance. To illustrate this point, Figure 9.13 compares data obtained in an anechoic chamber near a thin barrier placed on an absorbing surface of thickness 0.015 m with predictions of the Hadden and Pierce

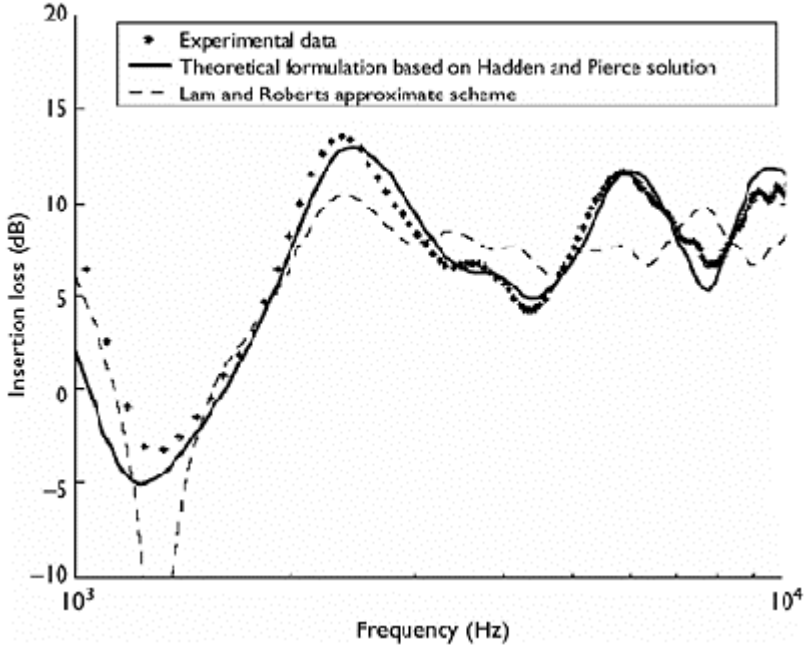

Figure 9.13 Comparison of laboratory data (points) with predictions obtained from the Hadden and Pierce solution (solid line) and the Lam and Roberts approximate scheme (broken line) for a barrier placed on an impedance ground. The source is located at 0.355 m from the barrier and at 0.163 m above the ground. The receiver is placed at 0.342 m from the barrier and 0.198 m above the ground. The ground is modelled as a Delany and Bazley hard backed layer (3.1, 3.2) with effective flow resistivity 9000 Pa s m^{-2} and (known) layer thickness of 0.015 m.

formula and Lam and Roberts approximate scheme. It is obvious that predictions obtained by using the Hadden and Pierce formula agree well with the experimental observations. On the other hand, while the Lam and Roberts model predicts the general trend of the insertion loss spectrum, it does not predict its magnitude as well, particularly in frequency intervals where the ground effects are strong.

9.5 Noise reduction by a finite length barrier

All outdoor barriers have finite length and, under certain conditions, sound diffracting around the vertical ends of the barrier may be significant. The MacDonald solution (see section 9.2.2) has been adapted to include the sound fields due to rays diffracted around the two vertical edges of a finite length barrier [31]. There are other diffraction theories for the vertical edge effects which have met with varying degrees of success when compared with data [32, 33]. In this section,

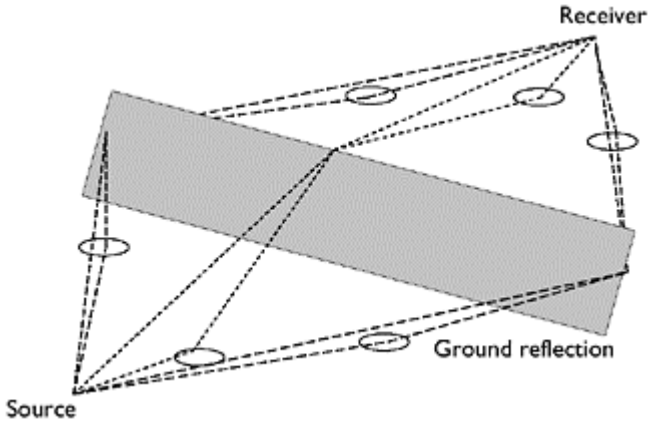

Figure 9.14 Eight ray paths associated with sound diffraction by a finite length barrier.

a more practical method is described [30]. The accuracy of this approach has been verified [34]. Figure 9.14 shows eight diffracted ray paths contributing to the total field behind a finite length barrier. In addition to the four 'normal' ray paths associated with diffraction at the top edge of the barrier (see Figure 9.7), four more diffracted ray paths from the vertical edges, including two ray paths each from either side, have been identified. In principle, there are reflected-diffracted-reflected rays also which reflect from the ground twice but these are ignored. This is a reasonable assumption if the ground is acoustically soft. The two rays at either side are, respectively, the direct diffracted ray and the diffracted-reflected ray from the image source. The reflection angles of the two diffracted-reflected rays are independent of the barrier position. These rays will either reflect at the source side or on the receiver side of the barrier depending on the relative positions of the source, receiver and barrier. We illustrate both possibilities in Figure 9.14. The total field is given by

$$P_T = P_1 + Q_s P_2 + Q_R P_3 + Q_s Q_R P_4 + P_5 + Q_R P_6 + P_7 + Q_R P_8, \tag{9.39}$$

where P_1-P_4 are those given in (9.34 a–d), for diffraction at the top edge of the barrier. The contributions from the two vertical edges E_1 and E_2 are $P_5 \equiv P(S_g, R_g, E_1)$, $P_6 \equiv P(S_i, R_g, V_1)$, $P_7 \equiv P(S_g, R_g, V_2)$ and $P_8 \equiv P(S_i, R_g, E_2)$ respectively. The spherical wave reflection coefficient Q_R is used for P_6 and P_8 as the reflection is assumed to take place at the receiver side but Q_s should be used instead if the reflection happens at the source side.

Although we can use any of the more accurate diffraction formulas described in section 9.2 to compute P_1-P_8, a simpler approach, following Lam and Roberts [30], is to assume that each diffracted ray has a constant phase shift of $\pi/4$ regardless of the position of source, receiver and diffraction point. Thus the empirical formulations described in section 9.3 can also be used to compute the amplitudes of the diffracted rays. Indeed,

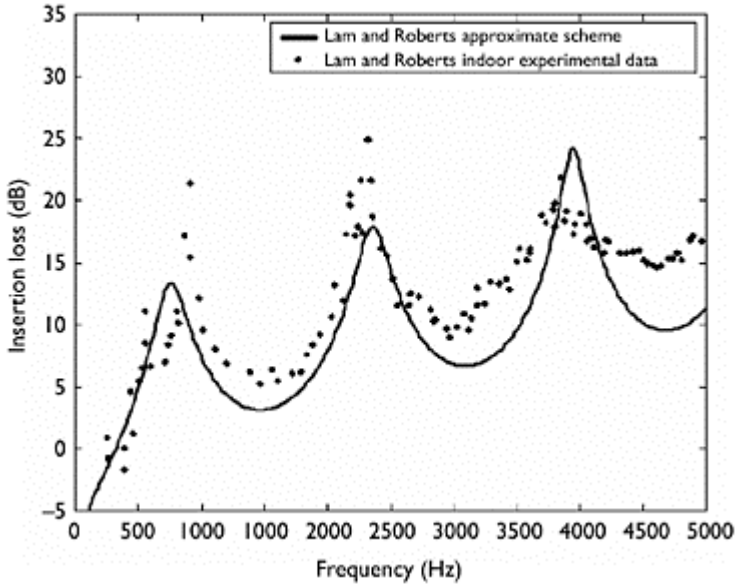

Figure 9.15 Comparison between laboratory data for the insertion loss of a barrier (0.3 m high and 1.22 m long) on hard ground and predictions using the Lam and Roberts approximate scheme [30]. The source was 0.033 m high and 1.008 m from the barrier. The receiver was on the ground and 1.491 m from the barrier.

Muradali and Fyfe [34] compared the use of the Maekawa chart, the Kurze-Anderson empirical equation and the Hadden-Pierce analytical formulation with a wave-based Boundary Element Method (BEM). Predictions of the ray-based approaches show excellent agreement with those of the relatively computationally intensive BEM formulation.

In Figure 9.15, data obtained by Lam and Roberts (figure 3 in [30]) are compared with predictions using their proposed approxi mation scheme. In their studies, the measurements were conducted over a hard ground with the barrier height of 0.3 m and length of 1.22 m. The source was located at 1.009 m from the barrier at the source side and 0.033 m above the ground. The receiver was situated at 1.491 m from the barrier at the receiver side with the microphone placed on the ground. Although the data shown in Figure 9.15 are the same as used by Lam and Roberts, the predicted spectrum of the insertion loss is calculated by our own computer program. Predictions based on other numerical schemes detailed in sections 9.2 and 9.3 are not shown because they tend to give similar results to the Lam and Roberts predictions.

9.6 Adverse effect of gaps in barriers

When the transmission of sound through the barrier is negligible, the acoustic field in the shadow region is mainly dominated by the sound diffracted around the barrier. However, in some cases, leakage will occur due to shrinkage, splitting and warping of the panels, and weathering of the acoustic seals. The problems of shrinkage and splitting are particularly acute for noise barriers made of timber. Sometimes gaps are unavoidable since spaces are required, for example, for the installation of lamp posts in urban districts. Watts [35] has investigated the resulting sound degradation of screening performance due to such leakage. He used a 2-D numerical model based on the BEM to predict the sound fields behind barriers of various heights with different gap widths and distributions. The A-weighted sound leakage increases as the gap size increases. Also, he reported that (a) sound leakage is more significant in region closed to barrier and (b) there are no significant leakage effects of noise from heavy vehicles. It should be noted that only horizontal gaps can be included in his two-dimensional boundary element model. Here we outline a recent theory developed by Wong and Li [36] and show that their predictions of the effects of barrier leakages agree reasonably well with data from laboratory and outdoor experiments.

Consider the barrier diffraction problem shown in Figure 9.16.

Based on the Helmholtz integral formulation, Thomasson [37] derived an approximate scheme for the prediction of the sound field behind an infinitely long barrier. The solution for a thin rigid screen is given by

$$\phi(\mathbf{r_R}, \mathbf{r_S}) = \phi_L(\mathbf{r_R}|\mathbf{r_S}) - 2\iint_{S_0} \phi_L(\mathbf{r_0}|\mathbf{r_S}) \frac{\partial \phi_L(\mathbf{r_R}|\mathbf{r_0})}{\partial x_R} dS \qquad (9.40)$$

barrier (small solid circles). The impedance of the fibreglass layer was predicted by using the Delaney and Bazley one-parameter model (3.2) and assuming an effective flow resistivity of 40 kPa s m $^{-2}$. Good agreement between the predicted and measured insertion losses is evident.

In this way, L'Espérance *et al*. have shown that the application of sound absorption materials on the barrier façade can lead to a significant improvement in the barrier's performance. However, Hayek [44] has suggested that barrier absorption is less effective in reducing the diffracted noise in the shadow zone where ground absorption is the most dominant factor in determining the acoustic performance of the barrier. It remains important to investigate the effectiveness of using absorptive screens in protecting receivers from excess noise particularly for the case in urban environments where multiple reflections and scattering between surfaces are prevalent.

9.8 Other factors in barrier performance

Although there are many other factors that may affect the barrier effectiveness in shielding receivers from excessive noise, in this section we shall address the two issues concerning meteorological effects and the influence of barrier shape that are of current research interest and give a brief review of the salient points.

9.8.1 Meteorological effects

In the barrier diffraction models described earlier, atmospheric conditions have been assumed to be steady and uniform. However, meteorological effects, such as temperature and wind velocity gradients, play a very important role in determining the acoustic performance of barriers. As a result of atmospheric refraction, barrier effectiveness is expected to be reduced in the downwind direction but enhanced in the upwind direction. By means of full-scale measurements conducted in the 1970s, Scholes *et al*. [45] demonstrated such wind effects on the acoustic performance of a noise barrier. Salomons [46] was among the first to study the effect of an absorbing barrier in a refracting medium by using a Parabolic Equation (PE) formulation. He assumed an absorbing barrier in his PE model and set the pressure at the grid points representing the barrier to zero. Thus, the part of the sound that falls on the barrier is stopped. A minor conflict appears in his method. The enforced zero pressure on grid implies that the normal velocity on barrier is zero too. This is the boundary condition for rigid surface. On the other hand the PE, which assumes only forward propagation from source to receiver, does not allow any backscattering of waves by the barrier. Thus, the reflection from the barrier is ignored when computing the total diffracted field. Rasmussen [47] studied the diffraction of barrier over an absorbing ground and in an upwind condition both theoretically and experimentally. He used an approach rather similar to the fast field formulation to estimate effective distances from source to the barrier edge and from the barrier edge to receiver in an upwind condition. Then the uniform theory of diffraction [48] was used to compute the diffracted sound field in the shadow zone. It is questionable whether the barrier diffraction can be 'de-coupled' from the wind gradient effects in this way. Nevertheless, Rasmussen's numerical results agreed reasonably well with his 1:25 scale

model experiments. Muradali and Fy fe [49] have proposed a heuri stic method for modelling barrier performance in the presence of a l inear sound speed profi le. Their model combines the effects of the sound refracted over a barrier and the sound diffracted by a barrier. Geometrical ray theory is used to determine the ray paths and the diffracted wave effect is incorporated by using the modified Hadden-Pierce formula. Li and Wang [50] have proposed a novel method to simulate the effects of a noise barrier in a refracting atmosphere. They mapped the wave equation in a medium where the speed of sound varies exponentially with height above a flat boundary to that for a neut ral fluid above a curved surface. The barrier problem in an upward-refracting m edium is then solved by applying the sta ndard Boundary Elem ent Method over a curved surface in a homogeneous medium. Recently, Taherzadeh *et al*. [51] developed a hybrid scheme for predicting barrier in a downwi nd condition. Their numerical scheme is based on a combination of the boundary integral and FFP techniques in which the Green's function required in the boundary integral equations is evaluated by using the FFP formulation. Atmospheric turbulence is an i mportant factor in barrier perform ance since it causes scattering of sound into the shadow zone. Although experimental studies of the effects of atmospheric turbulence on t he acoustic performance of the barrier are rare, theoretical studies have been conducted by Daigle [52], Forssén and Ogren [53] and others quoted in these references. Some progress in modelling the acoustic performance of barri ers in a turbulent atmosphere using a substitute sources method has been reported by Forssén [54, 55]. Hybrid models have been proposed, i nvolving combinations of t he BEM with the PE, that enable effects of barriers, range-dependent impedance and turbulence to be taken into account [56, 57]. Rasmussen and Arranz [58] have appl ied the Gilbert *et al*. [59] approach, assuming weak atmospheric turbulence with a simple Gaussian distribution in the fluctuating velocity field, in a PE formulation to predict the sound field behind a thin screen in a scal e model experiment. The indoor experiments based upon a 1: 25 scaling ratio were conducted in a wind tunnel in which the agreement of num erical results and experimental measurements was very good. They concluded that the flow pattern associated with a speci fic noise barrier could be an important design parameter for improving the acoustic performance of barri ers. Improvements in computational speeds and resources have encouraged wider use of time domain models in acoustics. Recent work has been devoted to combining calculations employing time-dependent computational fluid dynamics with PE-based frequency domain calculations [60]. However, there are few studies to m easure or predict the velocity profiles and their associated turbulence accurate ly in the region close to a barrier on the ground and it remains a chal lenge to combine fluid dynamics and di ffraction models to establish an accurate scheme for predicting the acoustic effectiveness of screens under the influence of wind.

9.8.2 Effects of barrier shape

Most of the theoretical and experim ental studies found in literature are focused on a straight-edge barrier or a wedge. In fact , the shapes of barrier edges can affect their shielding efficiencies signifi cantly. Variations in the barrier shapes m ay be used to improve the shielding performance without increasing the height of barriers.

9.8.2.1 (a) Ragged-edge barrier

Wirts [61] introduced a type of barrier with non-straight top edge called 'Thnadners'. The saw-tooth Thnadners barrier consists of a number of large triangular panels placed side by side. Flattop Thnadners are similar to sawtooth Thnadners but each of the sharp corners at the saw-tooth top is flattened. Wirts suggested using the simplified Fresnel theory to calculate the sound fields behind Thnadners barriers. Results of his scale model experiments agreed with the proposed theory. The most interesting conclusions of his study are additional improvements on the shielding performance if some parts of the barrier are removed. Improvements are obtained at some receiver locations even if over 50% of the barrier surface areas are removed.

Ho *et al*. [62] conducted many scale model experiments and concluded that the acoustic performance of a barrier can be improved at high frequencies by introducing a random fluctuation to the height of the barrier, producing the so-called ragged-edge barrier. However, the poorer performance of the raggededge barrier at low frequencies was not explained. An empirical formula for the insertion loss of the ragged-edge barrier was obtained from the experimental results. The formula involves four parameters which are the frequency of the incident sound, the Fresnel number, the maximum height fluctuation from the average barrier height and the horizontal spacing between the height fluctuations.

Shao *et al*. [63] have proposed a 2-D model for a random edge barrier. Their models were based on the Rubinowics-Young formula which is a line integral method. The integration is performed along the random edge. They also conducted scale model experiments to validate their theoretical models. They concluded that the improvement could be obtained by introducing a random edge profile, especially at high frequencies. The insertion loss is controlled by the parameter of average barrier height and the variations of the randomness. In some cases, an improvement in the insertion loss can be obtained if the average height of a random edge barrier is smaller than the original straight-edge barrier.

9.8.2.2 (b) Multiple-edge barriers

After reviewing relevant previous experimental studies by May and Osman [64] and Hutchins *et al*. [65], Hothersall *et al*. [66] have used the BEM approach to study T-profile, Y-profile and arrow-profile barriers theoretically (see Figure 9.21). They concluded from their numerical simulation results and previous work that a multiple-edge profile barrier has better acoustical performance than a normal thin plane barrier of the same height. However, in most conditions, the Y-profile and arrow-profile barriers perform less efficiently than the T-profile barrier. The use of T-profile barrier can benefit

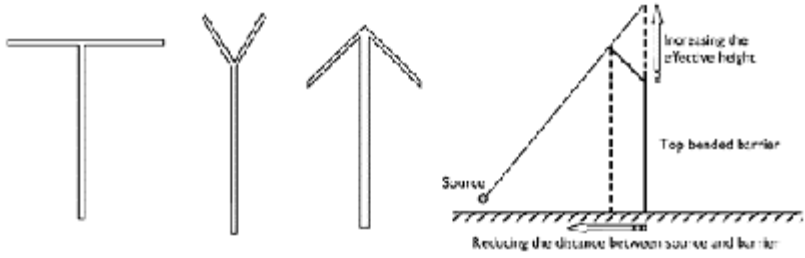

Figure 9.21 T-profile, Y-profile, arrow-profile and cranked (top-bended) barriers.

regions close to the barrier and close to ground. On the other hand, the height of the barrier is a dominant factor for the receiver located far away from the barrier and the top profile plays a less important role. The application of absorbent materials on the cap of T-profile has also been studied. A T-profile barrier with an absorptive cap can increase the insertion loss as long as the thickness of absorbent materials is thin. An excessively thick layer of sound absorbing materials can lead to a less efficient shielding. At present, only numerical tools, such as BEM, are used for study of the acoustic performance of the T-profile and multiple-edge barriers. Consequently, most of the theoretical studies are restricted to two dimensions.

Another type of multiple-edge barrier is the 'cranked' or top-bended barrier (see Figure 9.21) which is used increasingly in 'high-rise' cities. Jin *et al*. [67] have proposed an analytical method for the prediction of sound behind a top-bended barrier. They used a theoretical model based on the uniform geometrical theory of diffraction [48]. The total diffracted sound is calculated by sum ming multiple diffractions occurring at the top and corner points, at which convex and concave edges are formed. They concluded that the third and higher orders of multiple diffraction did not contribute significantly to the total diffracted sound and so these higher-order diffracted terms were ignored in their model. They compared the predicted insertion loss spectra between finite and infinite length barriers but some ripples caused by edge effects are evident in their predictions for the finite length barrier. Jin *et al*. used a commercially available BEM program me to compare with their analytical solutions for the 2-D case and obtained good agreement.

Okubo and Fujiwara [68] have suggested another design in which an acoustically soft waterwheel-shaped cylinder is placed on the top of a barrier. They studied its effects by using a 2-D BEM approach and conducted 3-D scale model experiments. They concluded that the insertion loss of barrier is improved by the cylinder but the effect is strongly dependent on the source frequency. Since the depth and opening angle of each channel influence the centre frequency, a suitable variation of the channel depth can flatten the frequency dependency and improve the overall performance of the A-weighted noise levels behind the barrier.

9.8.2.3 (c) Other barrier types

Wassilieff [69] has introduced the concept of picket barrier suggesting that traditional Fresnel-Kirchhoff diffraction is not applicable to a picket barrier at low-frequencies

because the wavelengths of the low-frequenc y sound are com paratively larger than the widths of the vertical gaps in the picket barrier. He added terms for a 'mass-layer' effect to the Fresnel-Kirchhoff diffraction theory to increase the accuracy of the model at low frequencies. Nevertheless, the original Fresnel-Kirchhoff diffraction theory gives better accuracy at the high-frequency region. He concluded that a careful adjustment of the picket gap can result in an improvement at certain low frequencies compared with a solid barrier. However, t he overall acoustic performance of barriers is reduced at other frequencies.

Lyons and Gibbs [70] have studied the acoustic performance of open screen barri ers, mainly the performance of louvre-type barrier at low frequency. Their model barrier consisted of vertical pickets, having a sound absorbing surface on one side, which were in two offset rows. The cavi ty left between two offset pickets is designed for better ventilation. They concluded that the side with the open area h as less in fluence on transmission loss at low-frequency sound. They also derived an empirical formula for the calculation of transmission loss of his louvre-type barrier with the dependent parameters being the overlapped area and t he cavity volume between two offset rows of pickets. They found that the leakage loss through two offset rows of pickets is relatively small at low frequency. As a refi nement of t his study, Viverios *et al*. [71] have devel oped a numerical model that was based on t he Fresnel-Kirchoff approximate scheme to estimate the transmission loss of a louvre barrier. Af ter incorporating the am plitude and phase changes due t o the absorbing materials within the louvre bladders, their model agreed reasonably well with measurements. Watts *et al*. [72] have used t he BEM formulation to study the acoustic performance of louvred noise barriers. Nevertheless, it seems that more theoretical and experim ental studies are requi red to develop a simple scheme for predicting the sound field behind open screen barriers.

A comprehensive summary of the efficiency of noise barriers of di fferent shapes can be found in the paper by Ishizuka and Fu jiwara [73]. The aut hors used t he boundary element method and st andard traffic noise spectrum to determine the broadband efficiency of several popular noise barrier shapes wi th respect to that predicted for an equivalent 3 m high plain noise screen. Thei r work shows t hat a com plex noise barrier edge, for example a Y-shape barri er or a barri er with a cylindrical edge, can yield a 4–5 dB improvement in the insertion loss. This is important when the increase in the barrier height is n ot practical or impossible. Figure 9.22 reproduced from [73] illustrates the change in the mean insertion loss relative to a st andard 3 m high, plane screen noi se barrier.

If a source of noise is clo se to the barrier, then the positive effect o f the complex barrier shape can becom e small in comparison with the effect of absorbi ng barrier treatment. This phenomenon has been i nvestigated, experimentally and num erically, by Hothersall *et al*. [74] who studied the performance of railway noise barriers. Reflecting

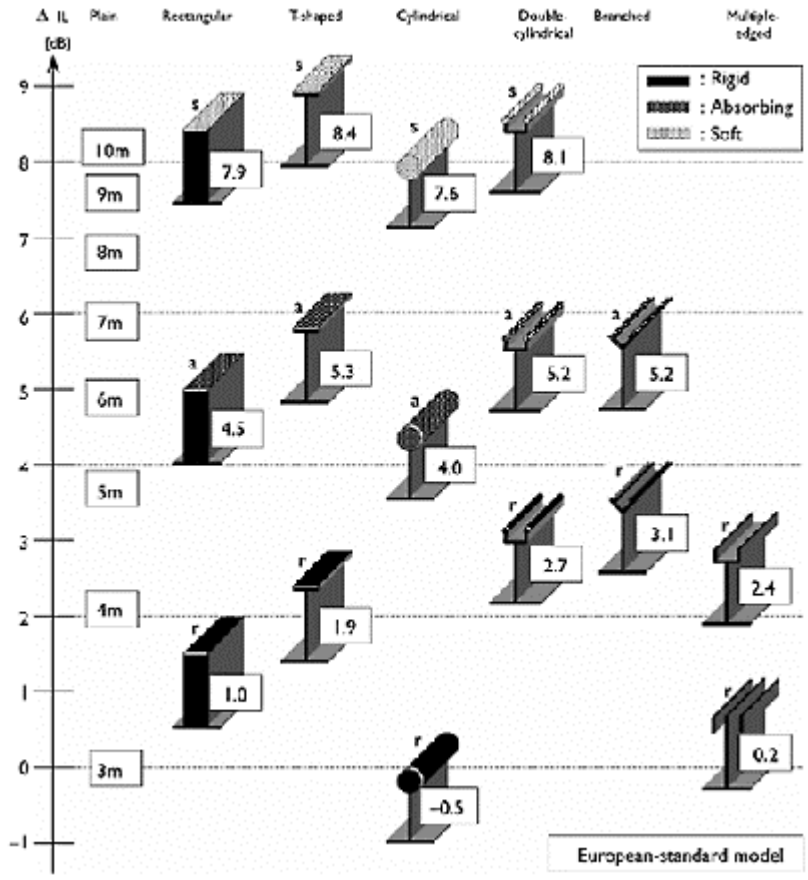

Figure 9.22 Predicted acoustic performance of traffic noise barriers of various shapes assuming a standard traffic noise spectrum. The figures indicate the relative change in the mean insertion loss relative to a 3 m plane screen [73]. Reprinted with permission from Elsevier.

and absorbing railway noise barriers of different shapes were positioned as close as possible to the train structure, within the limitations of the structure gauge (see Figure 9.23). The barrier shapes included a plain screen (a), a cranked screen (b), a parabolic screen (c), a multiple-edge noise screen (d) and a corrugated barrier (e).

It was found that the insertion loss values for a rigid screen were between 6 and 10 dB lower than those for a similar screen with absorbing treatment.

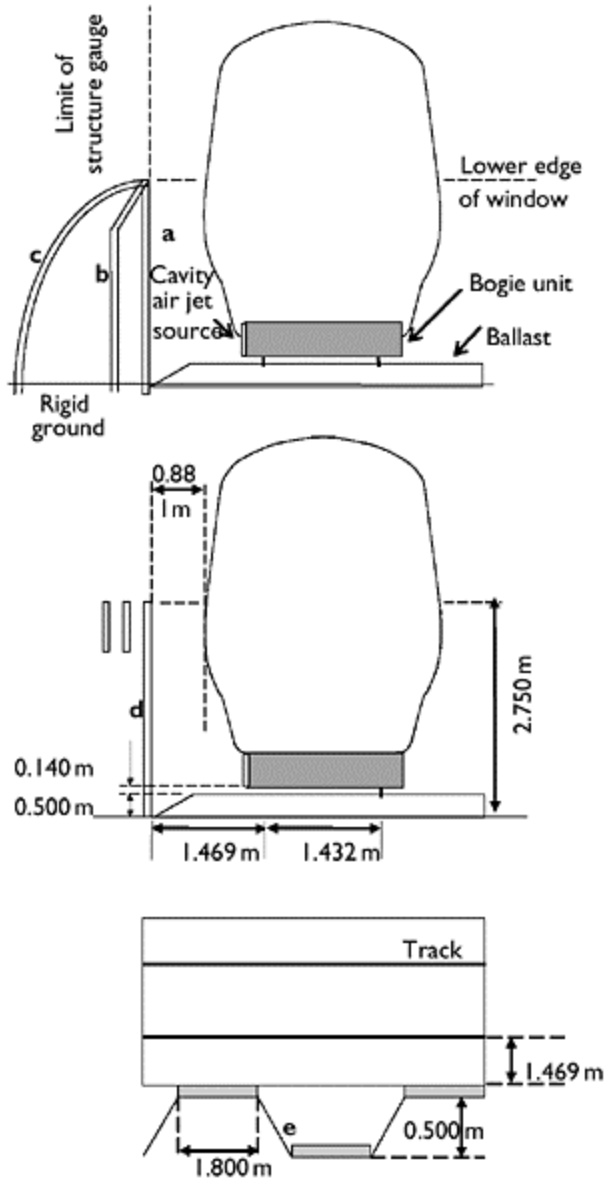

Figure 9.23 Configuration of the model and barrier cross-sections in a comparative study [74].

In a particular case, where a 1.5 m high plain screen was installed 1.0 m away from a passing railway carriage, the maximum predicted improvement in the average insertion loss due to the absorbing barrier treatment was 14 dB. On the other hand, any of the

modifications in the barrier shape, resulted in a less than 4 dB gain in the insertion loss compared with that of the basic plain screen of equivalent height [74].

9.9 Predicted effects of spectral variations in train noise during pass-by

Models for predicting the effects of noise control treatments rely heavily on the knowledge of the reference noise source spectrum. In road traffic noise studies, a standardized spectrum is used widely to account for the non-linearity in the emitted acoustic spectrum [75]. No similar standard exists at present to regulate the noise spectrum emitted by high-speed trains. Unlike noise from motorway traffic, which is a relatively stationary process, the noise spectrum of a train can vary significantly during its pass-by. The results of the work by Horoshenkov *et al*. [76] suggest that during the pass-by of a high-speed intercity train the variation of the sound pressure level (SPL), in the frequency range between 500 and 5000 Hz, can be as high as 20 dB sec^{-1}. It is common in many practical calculations to use the average spectrum for the whole pass-by. Indeed, several railway noise spectra have been compiled for such use [77, p. 175] . However, a likely drawback in adopting an average spectrum is the failure to model the distinctive time-dependent performance of noise control elements (e.g. noise barriers) during the pass-by of a train. In practice, the engineering measure of the *in situ* efficiency of a railway noise barrier, the broadband insertion loss, can vary considerably during the pass-by so that the perceived (subjective) acoustic efficiency of a noise control element is somewhat reduced. In this sense, one can argue that the noticeable fluctuations in the insertion loss during the train pass-by are subjectively more significant than the limited average barrier performance. This phenomenon may need to be given a careful consideration when the efficiency of expensive railway noise barrier schemes is assessed. Here we demonstrate that the variation in the reference noise source spectrum can result in a perceivable fluctuation of the noise efficiency of some noise barrier designs.

Figures 9.24 and 9.25 present typical narrow-band spectrograms measured for the passage of the Intercity 125 (diesel) and Intercity 225 (electric) trains respectively. The distances on the vertical axes in these Figures correspond to the time-dependent separation between the fixed receiver position on the ground and the varying position of the front locomotive in the train.

We have used the measured narrow-band spectrograms to determine the 1/3-octave band reference, time-dependent noise spectra which are required to model numerically the time-dependent insertion loss of three different barrier shapes: a plane screen, a screen with a quadrant of cavities at its upper edge (‘spiky top’) and a T-shape noise barrier. The ‘spiky top’ barrier has been designed to achieve its maximum efficiency